ADVANCED FUNCTIONAL MATERIALS

Supporting Information

for *Adv. Funct. Mater.,* DOI: 10.1002/adfm.202215155

Comprehensively Strengthened Metal-Oxygen Bonds for Reversible Anionic Redox Reaction

Congcong Cai, Xinyuan Li, Ping Hu, Ting Zhu, Jiantao Li, Hao Fan, Ruohan Yu, Tianyi Zhang, Sungsik Lee, Liang Zhou, and Liqiang Mai**

Supporting Information

Comprehensively Strengthened Metal-Oxygen Bonds for Reversible Anionic Redox Reaction

Congcong Cai, Xinyuan Li, Ping Hu, Ting Zhu, Jiantao Li, Hao Fan, Ruohan Yu, Tianyi Zhang, Liang Zhou, and Liqiang Mai**

Mr. C. C. Cai, Ms. X. Y. Li, Mr. P. Hu, Ms. T. Zhu, Mr. H. Fan, Mr. R. H. Yu, Mr. T. Y. Zhang, Prof. L. Zhou, Prof. L.Q. Mai
State Key Laboratory of Advanced Technology for Materials Synthesis and Processing, International School of Materials Science and Engineering, Wuhan University of Technology, Wuhan 430070, P. R. China

Prof. L. Zhou, Prof. L.Q. Mai
Hubei Longzhong Laboratory, Wuhan University of Technology (Xiangyang Demonstration Zone), Xiangyang 441000, Hubei, China.

Dr. J. T. Li
Chemical Sciences and Engineering Division, Argonne National Laboratory, 9700 South Cass Avenue, Lemont, IL 60439, USA

Dr. S. Lee
X-ray Science Division, Argonne National Laboratory, 9700 South Cass Avenue, Lemont, IL 60439, USA

Methods

Materials preparation. The $Na_{0.71}Li_{0.22}Al_xMn_{0.78-x}O_2$ (x = 0, 0.05, 0.1) samples were synthesized by a simple solid state reaction method. Typically, 7.1 mmol $NaNO_3$ (5 wt.% in excess), 2.2 mmol CH_3COOLi, 0.5 mmol $Al(NO_3)_3 \cdot 6H_2O$, and 7.3 mmol $Mn(CH_3COO)_2 \cdot 4H_2O$ were added into 40 mL deionized water with stirring to form a clear solution. The water was evaporated at 100 ℃ and further dried at 120 °C for 3h. After grinding, the precursors were heated to 500 ℃ for 2 h and 800 °C for 10 h in air. Then, the sample was cooled down to 500 °C at 1 °C min^{-1} and naturally to room temperature, and stored in an Ar-filled glovebox.

Characterization. X-ray diffraction (XRD) was performed on a Bruker D8 Advance X-ray diffractometer with a Cu Kα X-ray source (λ = 1.5406 Å). The data were refined by a TOPAS software. Scanning electron microscopy (SEM) images were collected on a JEOL-7100F microscope at 20 kV. The High-angle annular dark-field scanning transmission electron microscopy (HAADF-STEM) and the energy-dispersive spectroscopy (EDS) mapping were conducted in Titans Themis. Raman spectra were recorded using a Horiba LabRAM HR Evolution with an excitation laser with a wavelength of 532 nm. X-ray photoelectron spectroscopy (XPS) was carried out on a Thermo-Fisher Scientific-ESCALAB 250Xi equipped with an Al Ka monochromated X-ray source. X-ray absorption spectroscopy (XAS) measurements were collected at 12-BM-B at the Advanced Photon Source (APS) in Argonne National Laboratory. The radiation was monochromatized by a Si (111) double-crystal monochromator. Differential electrochemical mass spectrometry (DEMS) measurement was performed on a Hiden HPR 20.

Electrochemical measurements: The electrochemical performances were tested by assembling CR2016 coin cells in the Ar-filled glovebox. Sodium foil was used as both the counter and reference electrodes. The electrode was prepared by casting the slurry containing 70 wt.% of active materials, 20 wt.% of acetylene black, and 10 wt.% of polyvinylidene fluoride in N-methyl-2-pyrrolidone onto Al foil and dried at 100 ^oC in a vacuum oven overnight. 1.0 M $NaPF_6$ in propylene carbonate (PC) containing 5 % fluoroethylene carbonate (FEC) was used as the electrolyte and glass fiber was used as

the separator. The mass loading of active materials was 1 – 1.5 mg cm^{-2}. Galvanostatic charge/discharge (GCD) measurements were performed in a NEWARE battery test system within the potential range of 2.0 – 4.5 V (*vs.* Na^+/Na). Cyclic voltammetry (CV) test was conducted on CHI600E electrochemical workstations.

For *in-situ* tests, the electrodes consisted 80 wt.% of active materials, 10 wt.% acetylene black, and 10 wt.% of polytetrafluoroethylene (PTFE). The electrodes were charged to 4.5 V and then discharged to 2.0 V at 40 mA g^{-1}. For the *ex-situ* measurements, the electrodes were disassembled from the coin cell, washed with electrolyte solution repeatedly, and dried in an Ar-filled glove box.

Calculation method: First-principle calculations were performed by the density functional theory (DFT) using the Vienna Ab-initio Simulation Package (VASP) package.[1] The generalized gradient approximation (GGA) with the Perdew-Burke-Ernzerhof (PBE) functional was used to describe the electronic exchange and correlation effects.[2-4] Uniform G-centered k-points meshes with a resolution of 2π*0.04 $Å^{-1}$ and Methfessel-Paxton electronic smearing were adopted for the integration in the Brillouin zone for geometric optimization. The simulation was run with a cutoff energy of 500 eV throughout the computations. These settings ensure convergence of the total energies to within 1 meV per atom. Structure relaxation proceeded until all forces on atoms were less than 1 meV $Å^{-1}$ and the total stress tensor was within 0.01 GPa of the target value. To describe the on-site Coulomb interaction, the Hubbard U correction (GGA+U) was applied to the transition metals.[5] The value of U_{eff} (U-J) was set to 4.9 eV for Mn.[6] Besides, the bonding properties of Mn–O were revealed by the crystal orbital Hamilton population (COHP) analysis,[7] as implemented in the LOBSTER code.[8, 9] In order to construct $Na_{0.71}Li_{0.22}Mn_{0.78}O_2$ and $Na_{0.71}Li_{0.22}Al_{0.05}Mn_{0.73}O_2$, we used the P2-type $Na_2Mn_2O_4$ structure as the initial structure, and its space group was $P6_3/mmc$. Based on this structure, we established a 3*3*1 supercell to obtain $Na_{18}Mn_{18}O_{36}$, and then we replaced the transition metal Mn atom with 4 Li atoms and 1 Al atom, and then deleted 5 Na atoms to construct NLAM ($Na_{13}Li_4Mn_{13}AlO_{36}$). And the NLM ($Na_{13}Li_4Mn_{14}O_{36}$) structure was constructed without the introduction of Al atom.

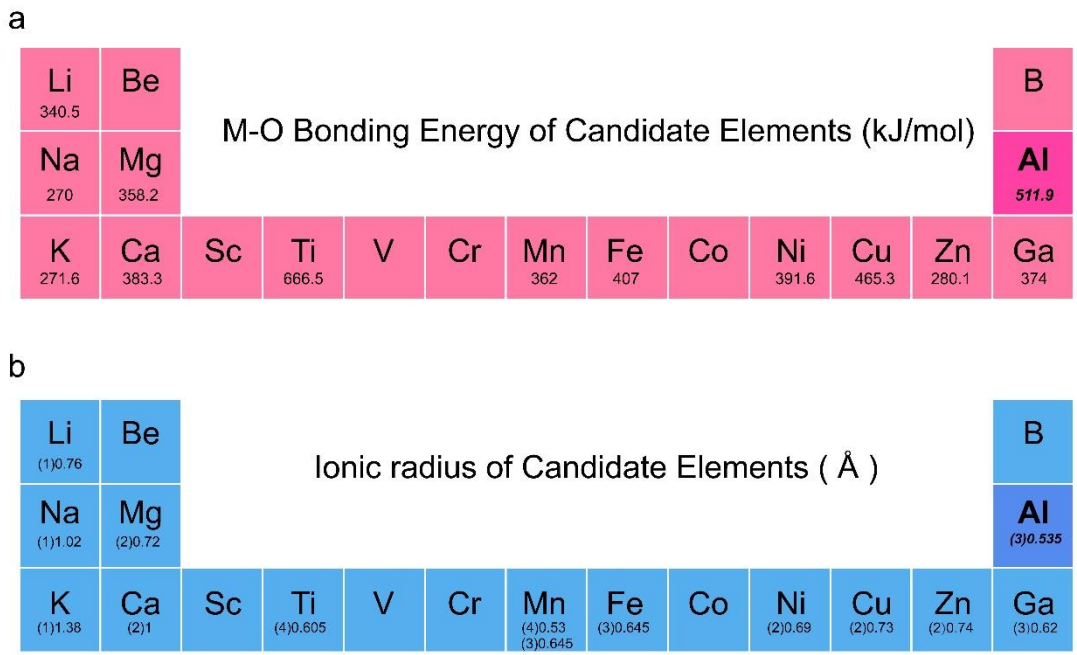

Figure S1. (a) M-O bonding energy and (b) ionic radius based on CRC Handbook of Chemistry and Physics (97th edition).[10, 11]

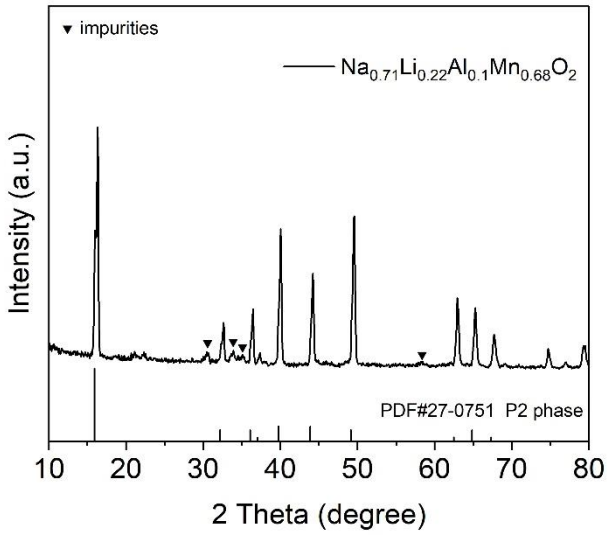

Figure S2. XRD pattern of 10 % Al doped sample.

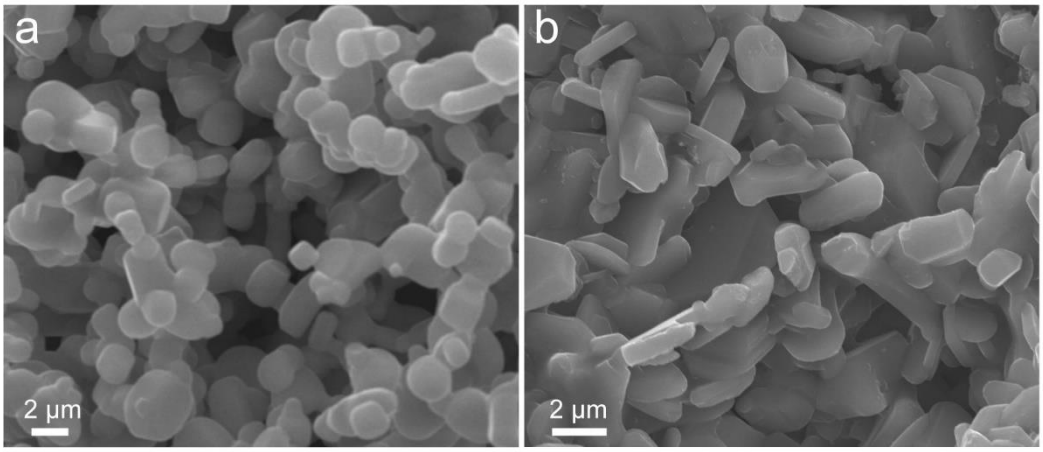

Figure S3. SEM images of (a) NLM and (b) NLAM.

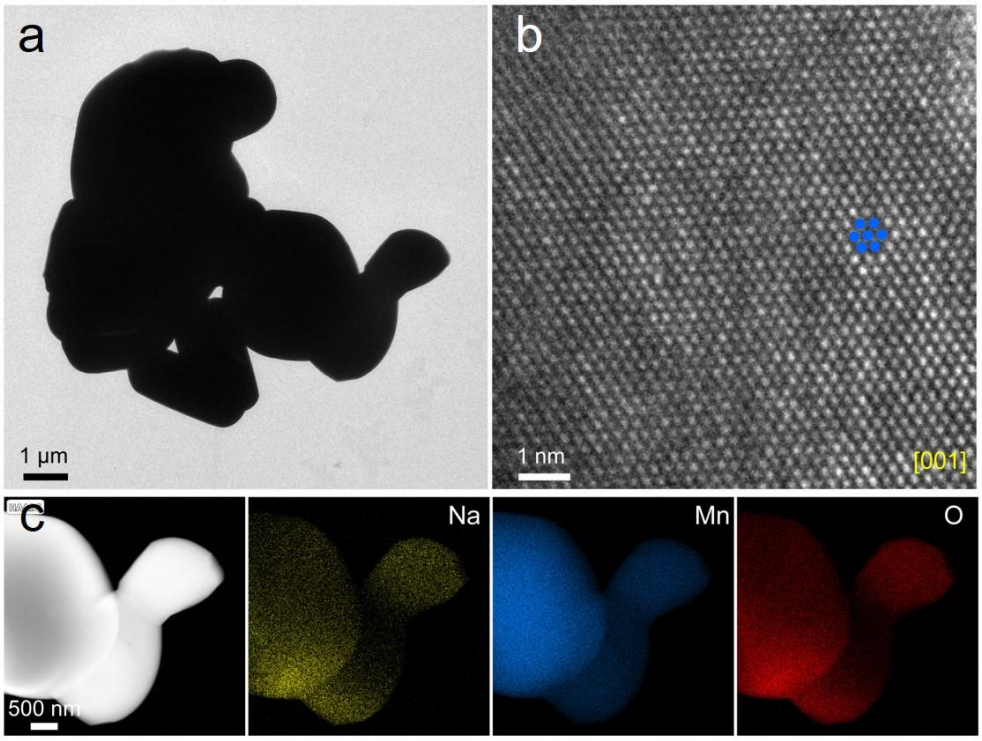

Figure S4. Structural characterization of NLM. (a) TEM image; (b) HRTEM image along [001] zone axis; (c) HAADF-STEM image with the corresponding EDS mappings.

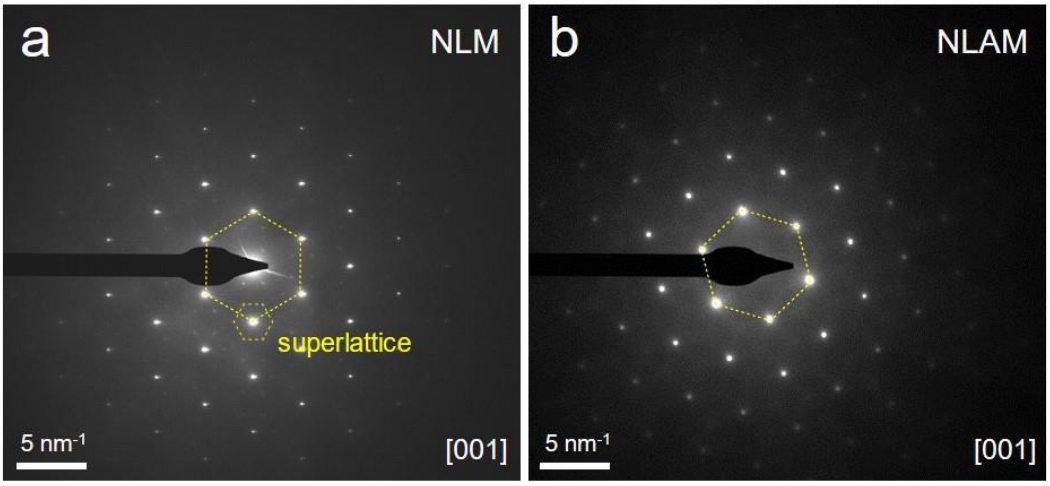

Figure S5. SAED pattern of (a) NLM and (b) NLAM.

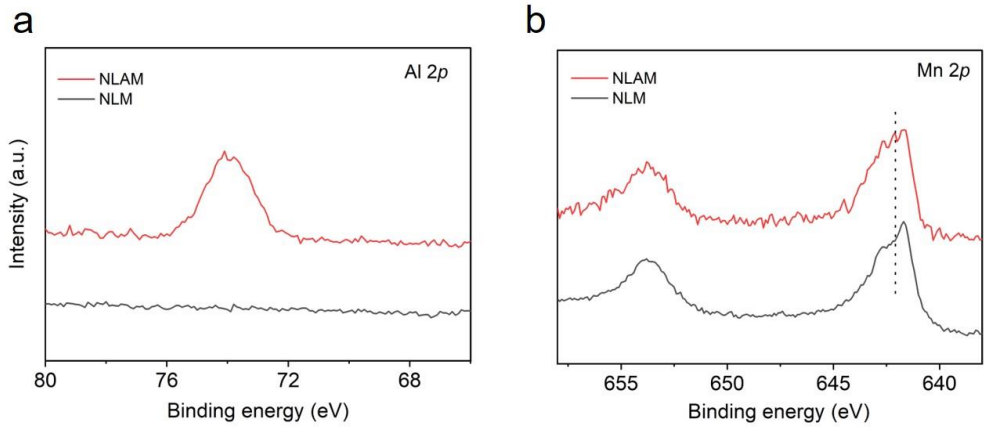

Figure S6. XPS spectra of (a) Al 2*p* and (b) Mn 2*p* for NLM and NLAM.

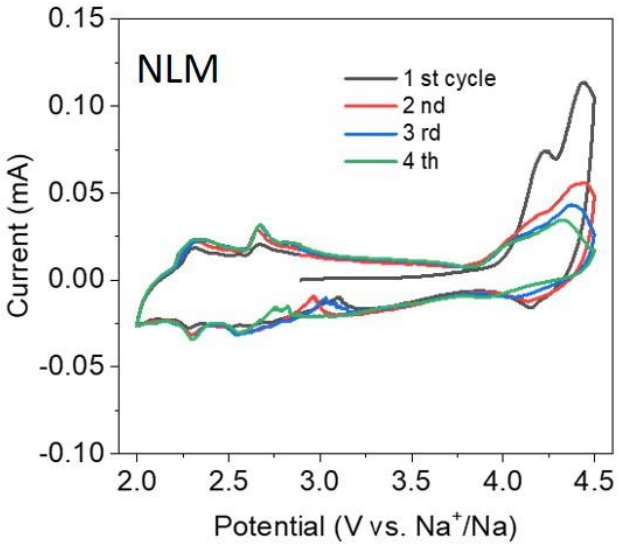

Figure S7. The first 4 CV curves of NLM.

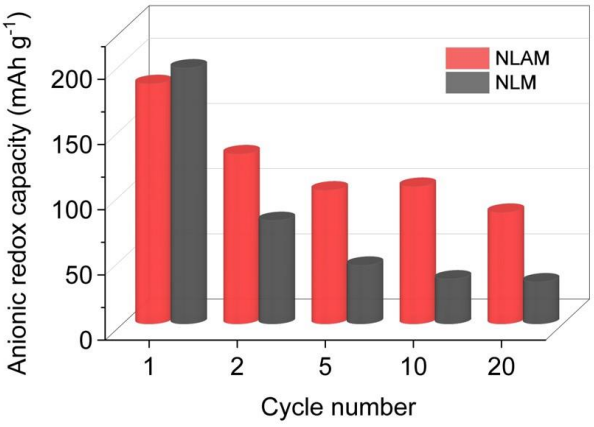

Figure S8. Comparison of the charge capacity above 4 V at different cycles at 20 mA g^{-1} of NLM and NLAM.

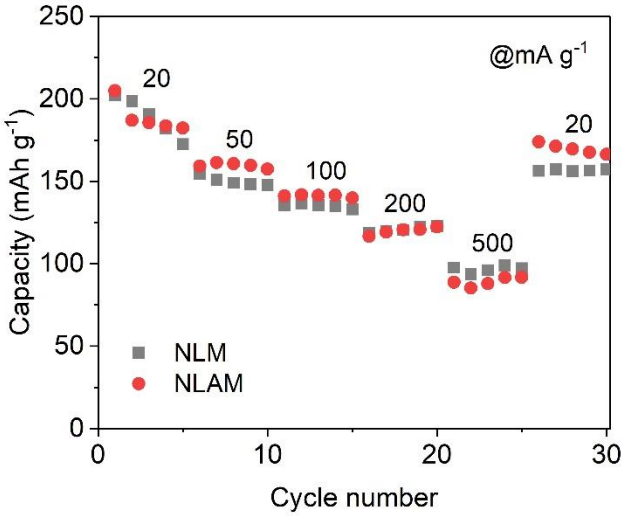

Figure S9. Rate performances of NLAM and NLM.

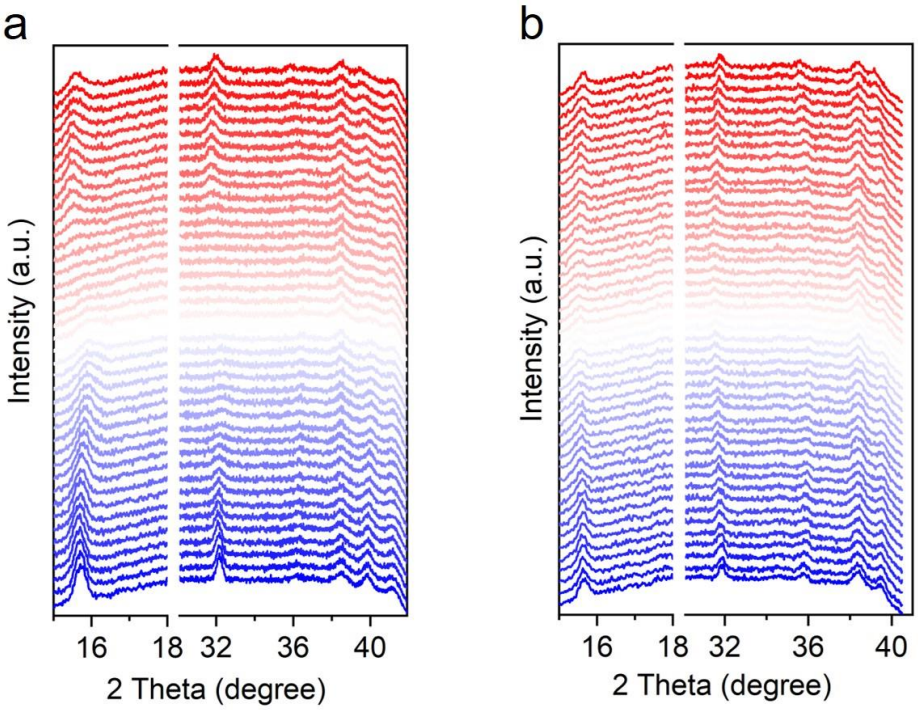

Figure S10. The corresponding *in-situ* XRD curves of (a) NLAM and (b) NLM at first cycle.

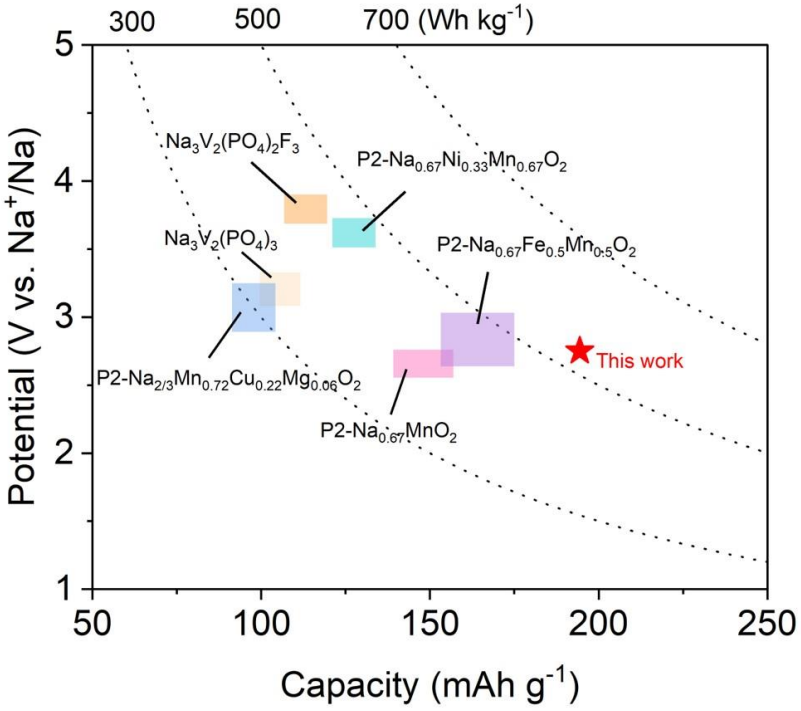

Figure S11. Comparison of the energy density of NLAM with other SIB cathode materials. [12-17]

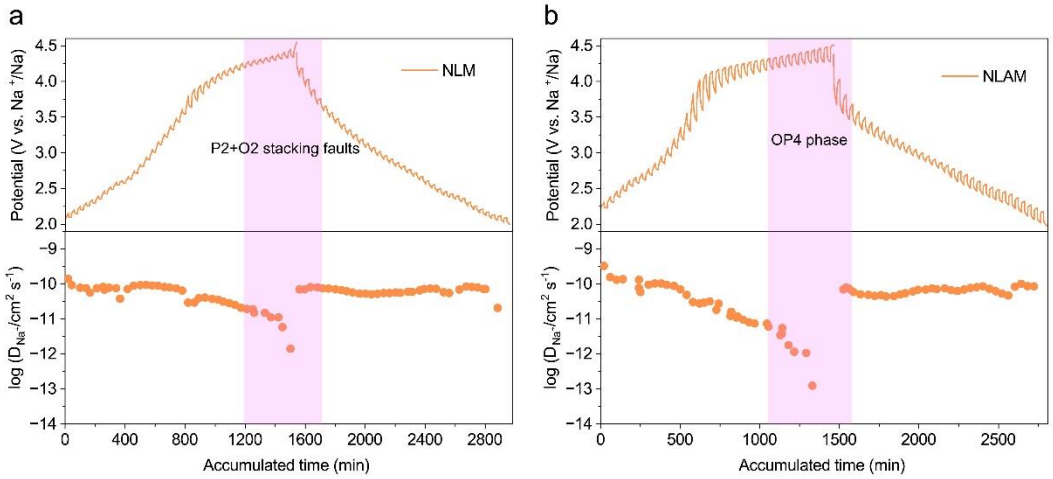

Figure S12. GITT tests and the calculated Na^+ diffusion coefficient (D_{Na^+}) for (a) NLM and (b) NLAM.

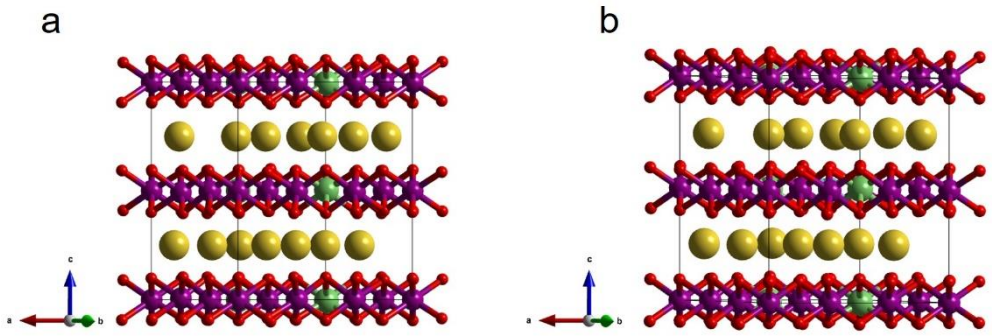

Figure S13. The optimized structures of (a) NLM and (b) NLAM (b). The yellow, green, purple, blue, and red balls represent Na, Li, Mn, Al, and O atoms, respectively.

Table S1. Crystallographic parameters of NLM obtained from XRD Rietveld refinement.

phase	Atom	site	*x*	*y*	*z*	Occ	R_{wp}	R_p
P2	Mn	2a	0	0	0	0.780	2.75%	1.93%
	Li	2a	0	0	0	0.220		
	Na1	2b	0	0	0.25	0.306(3)		
	Na2	2d	0.6667	0.3333	0.25	0.404(3)		
	O	4f	0.3333	0.6667	0.0951(3)	1		

$a = b = 2.8608(3)$ Å, $c = 11.0911(4)$ Å, $V = 78.609(3)$ Å^3.

Table S2. Crystallographic parameters of NLAM obtained from XRD Rietveld refinement.

phase	Atom	site	*x*	*y*	*z*	Occ	R_{wp}	R_p
P2	Mn	2a	0	0	0	0.730	2.12%	1.59%
	Li	2a	0	0	0	0.220		
	Al	2a	0	0	0	0.050		
	Na1	2b	0	0	0.25	0.268(2)		
	Na2	2d	0.6667	0.3333	0.25	0.442(2)		
	O	4f	0.3333	0.6667	0.0917(2)	1		

$a = b = 2.8640(2)$ Å, $c = 11.0666(3)$ Å, $V = 78.612(2)$ Å^3.

Table S3. Electrochemical performance comparison of NLAM and other layered cathodes with anionic redox reaction.

Layered oxide cathode	Voltage range	Specific capacity	Capacity retention	References
P2-type $Na_{0.773}Mg_{0.03}Li_{0.25}Mn_{0.75}O_2$	2-4.5 V	192 mAh g^{-1} (20 mA g^{-1})	~70 % 100 cycles at 20 mA g^{-1}	[18]
P2-type $Na_{0.67}Li_{0.21}Mn_{0.59}Ti_{0.2}O_2$	1.5-4.5 V	231 mAh g^{-1} (20 mA g^{-1})	~55 % 100 cycles at 200 mA g^{-1}	[19]
P2-type $Na_{2/3}Mg_{1/3}Mn_{2/3}O_2$	2-4.5 V	168 mAh g^{-1} (15 mA g^{-1})	80 % 100 cycles at 150 mA g^{-1}	[20]
P2-type $Na_{0.6}Mn_{0.65}Li_{0.15}Cu_{0.2}O_2$	2-4.5 V	88.5 mAh g^{-1} (12 mA g^{-1})	80 % 200 cycles at 120 mA g^{-1}	[21]
P2-type $Na_{2/3}Zn_{1/4}Mn_{3/4}O_2$	1.5-4.5 V	202.4 mAh g^{-1} (20 mA g^{-1})	67 % 50 cycles at 20 mA g^{-1}	[22]
O3-type $Na_{0.85}Li_{0.1}Ni_{0.175}Mn_{0.525}Fe_{0.2}O_2$	2-4.5 V	157 mAh g^{-1} (15 mA g^{-1})	88 % 100 cycles at 150 mA g^{-1}	[23]
This work	**2-4.5 V**	**194.4 mAh g^{-1} (20 mA g^{-1})**	**98.7 % after 100 cycles at 50 mA g^{-1} 98.6 % after 200 cycles at 200 mA g^{-1}**	

References

[1] G. Kresse and J. Furthmüller, *Comput. Mater. Sci.* **1996**, 6, 15-50.
[2] J. P. Perdew, K. Burke and M. Ernzerhof, *Phys. Rev. Lett.* **1996**, 77, 3865-3868.
[3] P. E. Blöchl, *Phys. Rev. B* **1994**, 50, 17953-17979.
[4] G. Kresse and D. Joubert, *Phys. Rev. B* **1999**, 59, 1758-1775.
[5] V. I. Anisimov, J. Zaanen and O. K. Andersen, *Phy. Rev. B* **1991**, 44, 943-954.
[6] B. Kim, K. Kim and S. Kim, *Phys. Rev. Mater.* **2021**, 5, 035404.
[7] R. Dronskowski and P. E. Bloechl, *J. Phys. Chem.* **1993**, 97, 8617-8624.
[8] V. L. Deringer, A. L. Tchougréeff and R. Dronskowski, *J. Phys. Chem. A* **2011**, 115, 5461-5466.
[9] S. Maintz, V. L. Deringer, A. L. Tchougréeff and R. Dronskowski, *J. Comput. Chem.* **2013**, 34, 2557-2567.

[10] Y.-R. Luo, Comprehensive handbook of chemical bond energies, CRC press, Boca Raton, FL, 2007.
[11] Q. Liu, Z. Hu, W. Li, C. Zou, H. Jin, S. Wang, S. Chou and S.-X. Dou, *Energy Environ. Sci.* **2021**, 14, 158-179.
[12] B. Pandit, M. T. Sougrati, B. Fraisse and L. Monconduit, *Nano Energy* **2022**, 95, 107010.
[13] L. Li, J. Zhao, H. Zhao, Y. Qin, X. Zhu, H. Wu, Z. Song and S. Ding, *J. Mater. Chem. A* **2022**, 10, 8877-8886.
[14] N. Yabuuchi, M. Kajiyama, J. Iwatate, H. Nishikawa, S. Hitomi, R. Okuyama, R. Usui, Y. Yamada and S. Komaba, *Nat. Mater.* **2012**, 11, 512-517.
[15] P.-F. Wang, Y. Xiao, N. Piao, Q.-C. Wang, X. Ji, T. Jin, Y.-J. Guo, S. Liu, T. Deng, C. Cui, L. Chen, Y.-G. Guo, X.-Q. Yang and C. Wang, *Nano Energy* **2020**, 69, 104474.
[16] P. F. Wang, Y. You, Y. X. Yin, Y. S. Wang, L. J. Wan, L. Gu and Y. G. Guo, *Angew. Chem. Int. Ed.* **2016**, 55, 7445-7449.
[17] W. Zuo, J. Qiu, X. Liu, B. Zheng, Y. Zhao, J. Li, H. He, K. Zhou, Z. Xiao, Q. Li, G. F. Ortiz and Y. Yang, *Energy Storage Mater.* **2020**, 26, 503-512.
[18] Y. Huang, Y. Zhu, A. Nie, H. Fu, Z. Hu, X. Sun, S. C. Haw, J. M. Chen, T. S. Chan, S. Yu, G. Sun, G. Jiang, J. Han, W. Luo and Y. Huang, *Adv. Mater.* **2022**, 34, 2105404.
[19] H. Xu, C. Cheng, S. Chu, X. Zhang, J. Wu, L. Zhang, S. Guo and H. Zhou, *Adv. Funct. Mater.* **2020**, 30, 2005164.
[20] K. Dai, J. Wu, Z. Zhuo, Q. Li, S. Sallis, J. Mao, G. Ai, C. Sun, Z. Li, W. E. Gent, W. C. Chueh, Y.-d. Chuang, R. Zeng, Z. Shen, F. Pan, S. Yan, L. F. J. Piper, Z. Hussain, G. Liu and W. Yang, *Joule* **2019**, 3, 518-541.
[21] J.-J. Fan, P. Dai, C.-G. Shi, C. Song, L. Wu, Y. Wen, L. Huang and S.-G. Sun, *J. Mater. Chem. A* **2020**, 8, 22346-22355.
[22] Y. Wang, L. Wang, H. Zhu, J. Chu, Y. Fang, L. Wu, L. Huang, Y. Ren, C. J. Sun, Q. Liu, X. Ai, H. Yang and Y. Cao, *Adv. Funct. Mater.* **2020**, 30, 1910327.
[23] Y. You, S. Xin, H. Y. Asl, W. Li, P.-F. Wang, Y.-G. Guo and A. Manthiram, *Chem* **2018**, 4, 2124-2139.